Prediction of Axis Shift Distortion during Circumferential Welding of Thin Pipes Using the Finite Element Method

A model is validated to predict axial and circumferential stress distribution when welding thin pipe

BY G. RAVICHANDRAN, V. P. RAGHUPATHY, N. GANESAN AND R. KRISHNAKUMAR

ABSTRACT. Axis shift distortion is one type of distortion encountered during the circumferential welding of large, thin pipes. The result of this is the loss of coaxiality of the pipes. This type of distortion is caused by the time lag in the solidification of various segments of weld metal around the circumference. The development of shrinkage forces in the weld metal especially in the axial direction is nonuniform due to the time lag, and this causes axis shift for the pipes. The development of a mathematical model using the finite element method for prediction of axis shift distortion in thin pipes is described in this work. Thermal analysis and subsequent elastic-plastic stress analysis for the pipe are performed using four-noded, bilinear degenerated shell elements. In addition to axis shift distortion, axial and circumferential stress distributions in the pipe are also determined by the model. The model is validated by conducting partial welding on the circumference of a thin pipe and measuring the transient thermal history and root opening at the bottom. Details of thermal and elastic-plastic analyses, welding trials, thermal and displacement results and axial and circumferential stress results are presented in this paper.

Introduction

Distortion is an inevitable result of welding and is an undesirable deviation in the design dimensions and shape of the component after welding. The root cause for the phenomenon is the nonuniform plastic deformation around the regions of the weld and contraction of the weld metal and plasticized zones during cooling. Depending on the shape of the component welded and the location and orientation of the weld, distortion occurs in several forms. During circumferential welding of thin shells, distortion occurs in the form of radial contraction in the weld plane and axis shift for the pipes. The two pipes, which are originally coaxial, lose the coaxiality after welding, and the axes of the pipes become shifted as shown in Fig. 1. This type of distortion is termed axis shift distortion.

Axis shift distortion is caused by the time lag between the thermal cycles at various segments of the weld metal along the circumference. If the time lag is great, then shrinkage of the weld metal along the axial direction will not be uniform, and this differential shrinkage leads to the axis shift distortion. Thus, intuitively it can be realized that for this form of distortion to occur, the time taken for the circumferential welding must be great. In addition, the pipe must have less stiffness to resist the shrinkage forces. Hence, this type of distortion will be experienced in the case of thin-walled, large-diameter pipes welded with conventional welding speeds. This type of distortion was faced during the fabrication of a nuclear steam generator shell and was reported by Gunathan, *et al.* (Ref. 1). The axis shift distortion was found to pose problems in achieving the required clearances between the subassemblies of 235-MW pressurized heavy water type steam generators. Thus, in places where accurate alignments are required, this form of distortion is highly undesirable.

An effective analysis of this type of distortion uses the finite element method, which incorporates various phenomena associated with welding. The analysis of the welding distortion must be of elastic-plastic type because the localized plastic deformation around the weld, which produces incompatible strains, is the prime cause for distortion in the pipes. As the plastic strain accumulates during the loading path, the accurate determination of plastic strains is possible only with a transient analysis with suitable time increments. The analysis cannot be carried out using axisymmetric elements, as the condition of axisymmetry assumes that the stress distribution is rotationally symmetric and neglects the differential shrinkage of the weld metal around the circumference. So the analysis should include the circumferential variation of stresses. There are many reports on ther-

KEY WORDS

Axis Shift Distortion
Residual Stresses
Circumferential Welding
Finite Element Method
Shell Element
Thin Pipes
Thermal Stresses
Thermal Cycles
Transient Deflection

G. RAVICHANDRAN and V. P. RAGHUPATHY are with Welding Research Institute, Bharat Heavy Electricals Ltd., Tiruchirapalli, India. N. GANESAN and R. KRISHNAKUMAR are with Indian Institute of Technology, Madras, India.

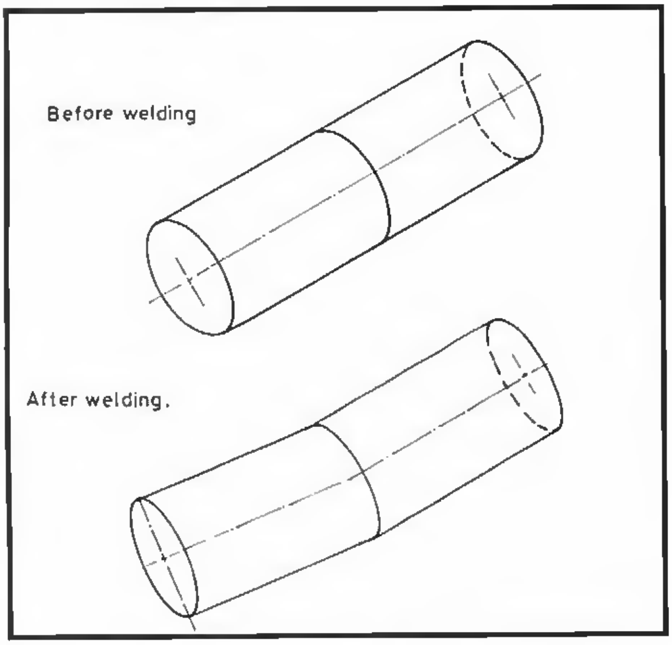

Fig. 1 — Axis shift distortion in a thin pipe.

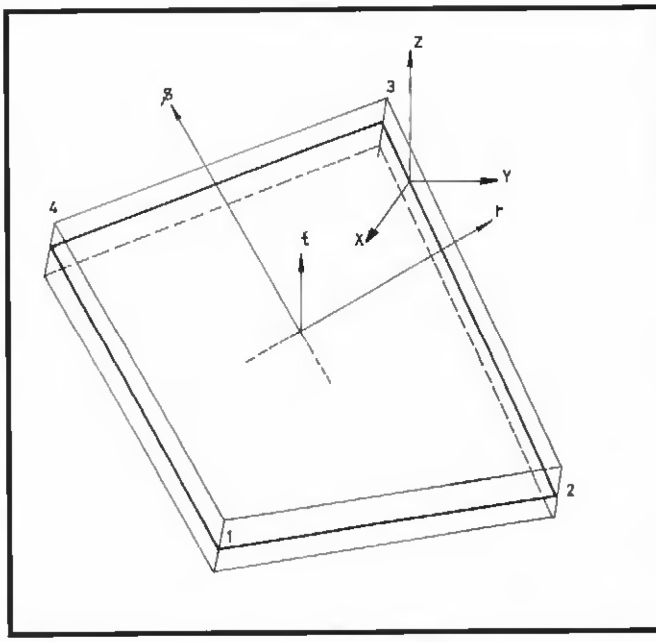

Fig. 2 — Four-noded shell element used in the thermal analysis.

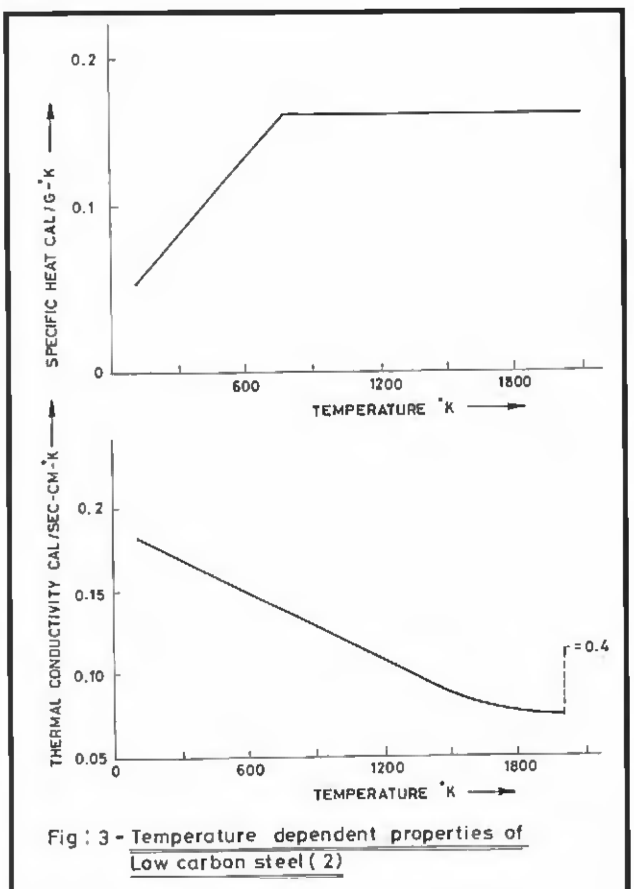

Fig. 3 — Temperature-dependent thermal properties of low-carbon steel (Ref. 3).

mal and elastic-plastic analyses on linear sections, but there are a few reports on the analysis of circumferential welds. A brief survey of the thermal and elastic- plastic stress analyses is presented below.

Friedman (Ref. 2), Krutz and Sergerlind (Ref. 3), Goldak, *et al.* (Ref. 4), and Elijah Kannatey-Asibu, Jr., *et al.* (Ref. 5), have successfully employed nonlinear transient finite element analysis for the prediction of thermal cycles in plates incorporating various phenomena, such as convection and radiation heat transfer, latent heat of fusion, temperature-dependent material properties and distributed arc heat, energy in the model. While Friedman has proposed a Gaussian model for the distributed arc energy, Goldak, *et al.*, has proposed a more accurate double ellipsoid model for the power density of the arc and has obtained the closest results. Goldak, *et al.* (Ref. 6), has compared the three-dimensional and two-dimensional transient thermal analyses and opines that while the 3-D analysis is very expensive, the 2-D in-plane analysis can be quite accurate for thin-section welds or regions farther from the arc where through thickness heat flow becomes insignificant. Karlsson, *et al.* (Ref. 7), who has analyzed the single-pass welding of a pipe using three-dimensional analysis, has reported that in the case of circumferential welding, due to the heat flowing backward from the beginning of the weld, the surroundings of the end of the groove become preheated. This preheating effect will be absent when the analysis for plates is extended for the case of pipes.

The elastic-plastic analysis using the finite element method has been reported by many leading researchers for linear sections. Friedman (Ref. 2) has presented a thermomechanical analysis on Inconel Alloy 600 weldment and has predicted weld-induced transient and residual stresses and distortion. Goldak, *et al.* (Ref. 8), have presented a nonlinear thermal elastic-plastic analysis for the computation of three-dimensional transient stresses, strains and displacement around a tack weld in a butt joint, and have shown that the assumption of plane strain condition in the stress model for a thick weldment is invalid. This conclusion when extended to the case of a pipe would imply that the choice of an axisymmetric model for the stress analysis

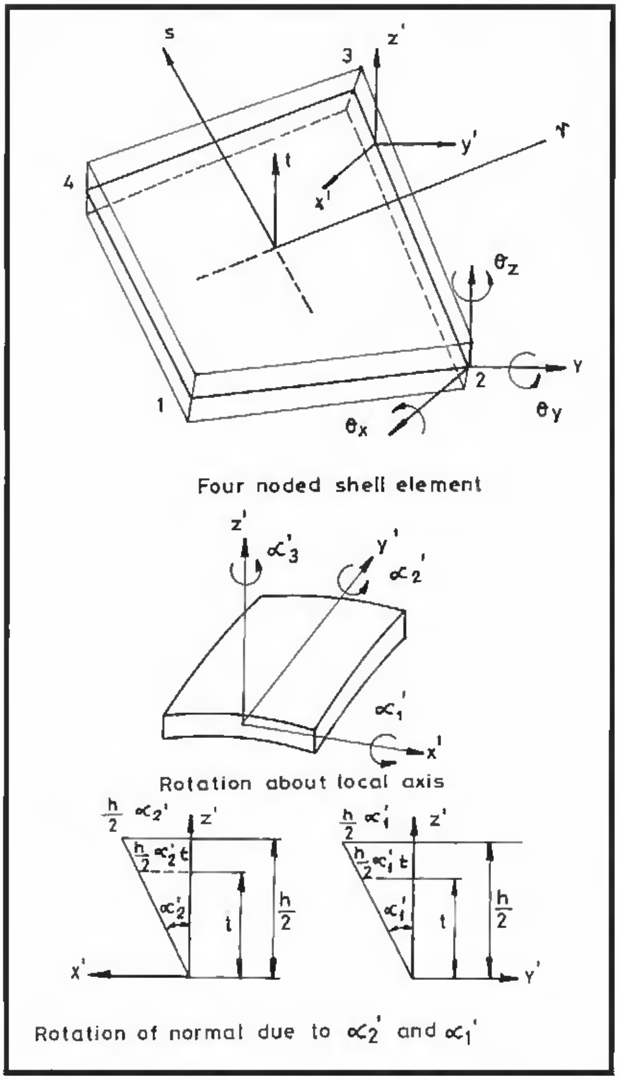

Fig. 4 — Degenerated shell element used in the stress analysis (Ref. 19).

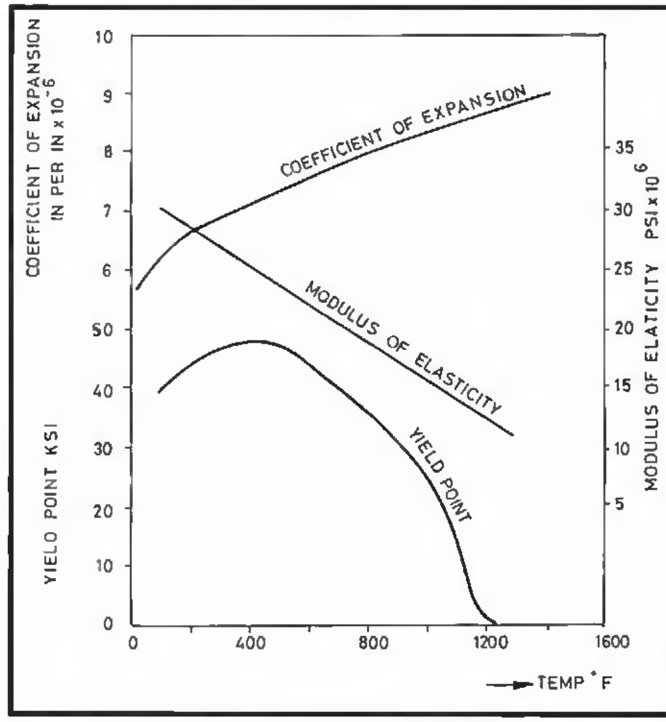

Fig. 5 — Changes in the physical and mechanical properties of steel with temperature (Ref. 23).

is also invalid. Leung, *et al.* (Ref. 9), has analyzed the residual stress distribution in a single-pass stainless steel weld and has described the development of a model indicating the necessary modeling features. Tekriwal and Mazumder (Ref. 10) have employed a rate-independent plasticity model with kinematic hardening rule and have discussed the choice of a suitable cut-off temperature for the analysis.

The stress analysis of circumferential welding of a pipe is more complicated than the analysis of a plate due to the geometric factor. Vaidyanathan, *et al.*, (Refs. 11, 12), has computed the final state of stress and radial displacements in circumferentially welded cylinders, by first determining the stress distribution in a plate and wrapping the final plate into a cylinder. Then the cylinder is allowed to deform, and the final configuration is determined from the condition that the elastic strain energy would be a minimum. Temperature distribution is obtained using a procedure similar to that described by Wells for a single-pass groove weld. The agreement between the experimental stress results in circumferentially welded thin hemispheres and the predicted values is found to be satisfactory

Rybicki, *et al.* (Ref. 13), has undertaken studies for the prediction of residual stresses during the welding of small-diameter 304 stainless steel pipes used mainly in the boiling water reactor piping systems. He has used the Rosenthal's analytical equation for the quasi-steady-state thermal solution with a point heat source. The residual stress analysis model is the finite element based elastic-plastic model with the assumption of axisymmetry. The model recognizes temperature-dependent elastic-plastic constitutive behavior, elastic unloading in the nonlinear stress strain range and changes in geometry due to deformation of each weld pass. There is a good correlation between the measured and computed temperatures, residual stresses and distortion.

Scaramangas (Ref. 14) has developed a computational model for predicting the local pattern of weld shrinkage stresses in multipass girth groove welds in pipes. He treats both thermal and elastic-plastic analysis as axisymmetric. The thermal model is based on the finite difference method with specified temperature distribution at the start of welding for the molten pool area. The stress-strain response to applied thermal load is evaluated from equations of equilibrium and compatibility using a stress function approach. The accumulation of plasticity is followed using the method of successive elastic solutions. The emphasis is on through-thickness stress distribution in the weld itself.

Chandra (Ref. 15), in his state of the art review paper, has described the closed form solutions and finite element solutions for the thermal and stress analyses. He mentions that in the finite element analyses, the condition of axisymmetry is generally assumed by researchers and for reasons of convenience and economy this approximation is considered satisfactory though the experimental evidence indicates that this is not generally the case. He has also presented some important results of experimental studies of residual stresses and has found that the axial variation of residual stress is very steep and the circumferential variation of axial stress is also significant, which contradicts the assumption of axisymmetry.

Jonsson, *et al.* (Ref. 16), has measured the axial and hoop stresses developed during welding with the help of strain gauges and has reported that the hoop stress component is reasonably rotationally symmetric, whereas the axial stress component is found to vary in the cir-

Fig. 6 — Close-up view of the tack-welded pipe.

Fig. 7 — Measurement of opening by feeler gauge.

cumferential direction. Lindgren, *et al.* (Ref. 17), has calculated the deformations and stresses during the welding of a shell structure. He has employed a degenerated shell element for the finite element method (FEM) analysis. The thermal analysis is carried out using analytical method and using the thermal elastic-plastic model, and the change in root width during welding of a plate is studied. His group has also calculated the residual stresses in a welded pipe and has compared the results with experimental data available in literature.

Josefson, *et al.* (Ref. 18), has discussed the development of stresses in a single-pass thin-walled groove-welded pipe. The calculated results from three different numerical FEM analyses, *viz.*, a rotationally symmetric, a fully three-dimensional and a shell model are compared with experimental results. He has reported that the stress field is not rotationally symmetric. Karlsson, *et al.* (Ref. 7), has analyzed the temperatures, stresses and deformations during single-pass welding of a pipe using a full three-dimensional model. The results show that the transient stress pattern in a section perpendicular to the weld interface is regular with respect to the hoop position except in the start and end regions of the weld. The hoop stresses in the weld are found to be of compressive nature.

From the survey, it is seen that with improvements in the power of computing, the assumption of axisymmetry for the analysis of pipe welding is no longer made and the trend is toward the use of shell elements and three-dimensional models. A full fledged three-dimensional model can be used for the analysis of axis shift distortion, but it will be very expensive and time consuming If the radial stress variation can be neglected, which

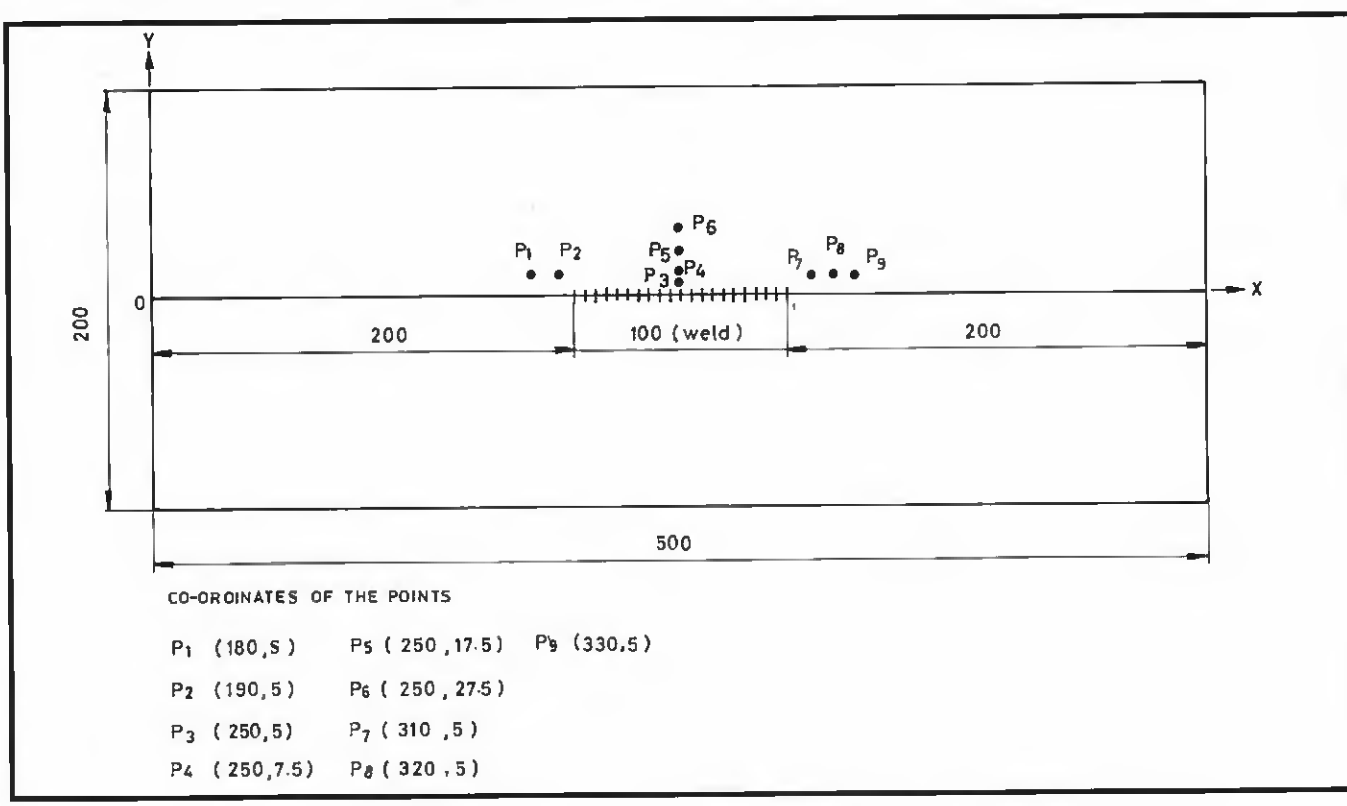

Fig. 8 — Locations of thermocouples in partially welded pipe.

Fig. 9 — Close-up view of the welding setup.

Fig. 10 — Opening of the gap at the bottom of the pipe.

is true for thin pipes, the analysis can be conducted using shell elements that will be cost effective. Hence, a FEM model using four-noded bilinear degenerated shell elements has been proposed for the prediction of axis shift distortion during welding of thin-walled pipes.

Finite Element Analysis

In the finite element analysis, the thermal and the mechanical aspects of the problem are uncoupled as the dimensional changes during welding are negligible and the mechanical work done during welding is insignificant compared to thermal energy change. Thus, the thermal analysis is conducted first and the complete thermal history at all points is determined for various time intervals. Subsequently, the stress analysis is conducted taking the nodal temperatures as input.

Thermal Analysis

The thermal analysis is conducted using a four-noded bilinear degenerated shell element, which is shown in Fig 2. The element is adapted from the one proposed by Kanok-Nukulchai (Ref. 19) for stress analysis. The assumption in the use of the element is that the heat flow normal to the midsurface is zero. At the midsurface of the element, an orthogonal set of local coordinate axes is constructed and, using the local coordinates of the nodes, the elemental calculations are carried out. The governing transient heat flow equation in the FEM is written as (Ref. 20)

$$[C]\{dT/dt\} + [K]\{T\} = \{F\}$$

where [C] = the thermal capacitance matrix;
[K] = the thermal conductivity matrix; {F} = the thermal load matrix; and t = time.

The physical properties required for the calculation of the two matrices, *viz.*, the thermal conductivity and the specific heat, are assumed to be temperature dependent. The material of the pipe is taken to be carbon steel, and the temperature dependency of the physical properties for the material is given in Fig. 3 (Ref. 3). The nodal arc heat is obtained by assuming that the arc heat distribution is as per Gaussian distribution (Refs. 2, 3). At each time interval, the nodes that receive the arc heat are identified and the corresponding heat values are calculated. The radiation and convection heat losses and the latent heat effects are accounted for in the model. The nodal temperatures are calculated for various time intervals from the temperature data for the previous time step through Galerkin's time stepping scheme. The time interval is kept constant during the welding phase. When the arc travels around the circumference, and in the cooling phase, the time steps are progressively increased as the thermal gradient slows down.

Stress Analysis

Analysis Using Degenerated Shell Element

The elastic-plastic stress analysis is

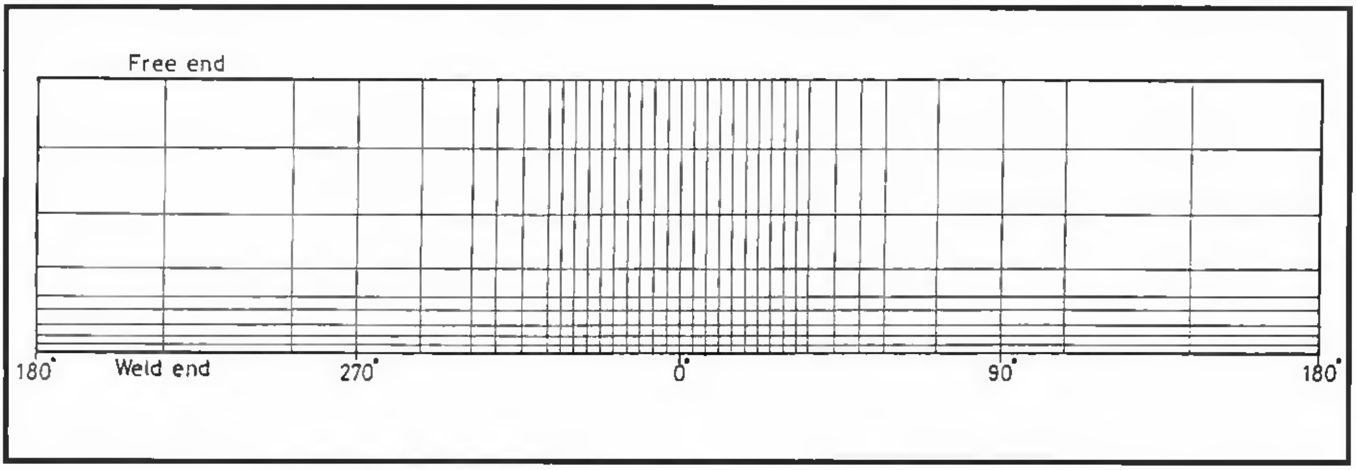

Fig. 11 — Discretization of the partially welded pipe (developed view).

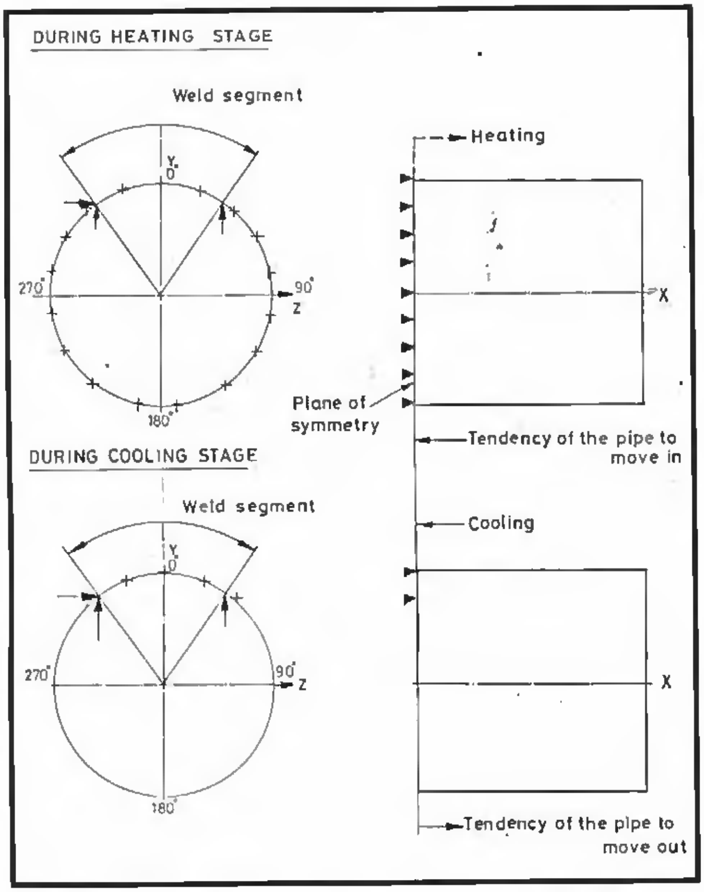

Fig. 12 — Boundary conditions employed for the partially welded pipe.

conducted with the help of a four-noded bilinear degenerated shell element having six nodal degrees of freedom as shown in Fig. 4, which is presented by Kanok-Nukulchai (Refs. 19, 21, 22). The degrees of freedom include three translations along the axes and three rotations about the axes. The element is based on Mindlin's theory, which assumes that straight lines originally normal to the midsurface before deformation remain straight but not necessarily normal to the deformed midsurface. Thus, the average rotation of the section may be taken as the rotation in which normals remain perpendicular to the midsurface plus an additional rotation due to transverse shear. In addition, the element assumes that the stresses normal to the midsurface are zero. Thus, the element assumes five stress components in the local coordinates, *i. e.*, σ_x, σ_y, τ_{xy}, τ_{yx} and τ_{zx}.

The displacement variation is expressed as a function of nodal displacements and the relative displacements produced by the rotation of the normal at the nodes. At a point on the midsurface, an orthogonal set of local axes is constructed as shown in Fig. 4, and the relative displacement components along the three axes in the local coordinates produced by the normal rotations are determined. The element stiffness matrix is constructed after determining the bending and membrane effects and the transverse shear effects. A lower order of integration is employed in the computation to avoid the shear locking effect (Ref. 19). Appropriate boundary conditions are assumed to prevent the rigid body motion of the pipe.

Elastic-Plastic Analysis

The elastic-plastic analysis is performed assuming that isotropic hardening rule is obeyed by the material. The model assumes von Mises equivalent stress for checking the condition of yielding and as-

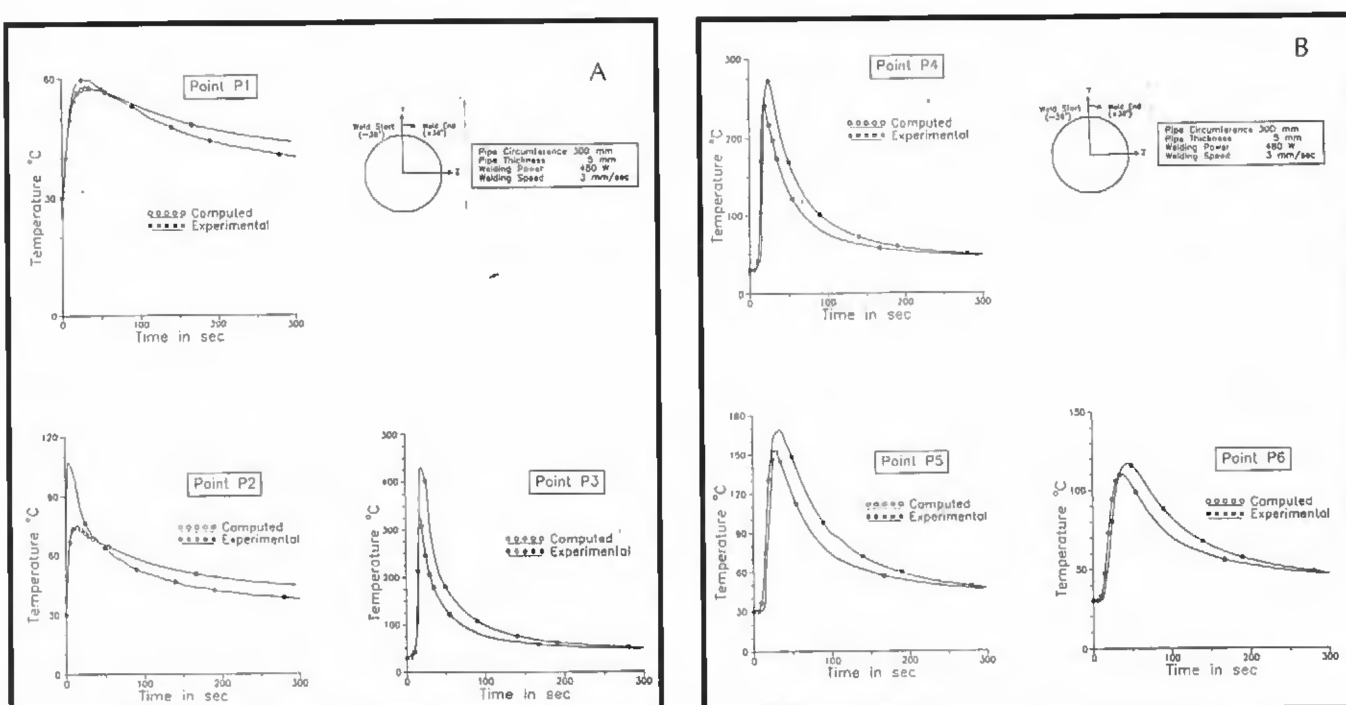

Fig. 13 — A — Comparison of thermal cycles in the partially welded pipe; B — comparison of thermal cycles in the partially welded pipe.

sociated flow rule for relating plastic strain and stress. The total strain increment experienced by the weldment is the summation of the thermal, elastic and the plastic strain increments. The constitutive equation is written in the form

$$[K]\{d\} = \{F\}$$

where $[K]$ = the element stiffness matrix given by $\int [B]^T \cdot [D_p] \cdot [B]\, dV$; $[B]$ = the strain displacement matrix; $[D_p]$ = the elastic plastic stress strain matrix; $\{d\}$ = the nodal displacements for the load step; F = the nodal thermal forces given by $\int [B]^T \cdot [D_p] \cdot \{\alpha\, dT\}\, dV$; α = the coefficient of thermal expansion in mm/(mm °C); dT = the incremental temperature for the load step in °C.

In the model, the material of the pipe is taken as carbon steel and the temperature dependency of the material properties are assumed as given in Ref. 23, which is shown in Fig. 5. The yield strength of the material is assumed to be zero above 750°C (1382°F) and the Young's modulus is assumed to be zero above 1190°C (2174°F). However, for the formulation of the stiffness matrix, a small value is assumed for the Young's modulus when the temperature exceeds 1190°C as the assumption of zero value leads to errors in computation. The ratio of plastic modulus to Young's modulus is assumed to be constant at all temperatures as suggested by Leung, *et al.* (Ref. 9). If the temperature of the element exceeds 1540°C (2804°F), then the stress and strain are assumed to be zero. On resolidification, the material would be damage free.

The analysis is conducted for a number of time steps from the start to the end of welding. Within each increment, the above analysis is performed and the displacements and stresses are determined through the Newton–Raphson iterative scheme. For the first iteration, the stiffness matrix is calculated on the basic of elastic assumption only and if the equivalent stress at any Gauss point exceeds the yield strength at that temperature, then the elastic-plastic stiffness matrix is recalculated and the displacements and stresses are determined through the iterative scheme. The iterations are repeated until convergence is achieved. For checking the convergence, residual forces and residual work done are checked against the values determined at the beginning of the step. If the residual values are within 0.1% of the original values, then convergence is assumed to be achieved. The limit of 0.1% has been suggested by Tekriwal and Mazumder (Ref. 10) for getting accurate results.

In the analysis, the thermal loads above a cut-off temperature are assumed to be zero, and the value of the cut-off temperature is 750°C, whereas Goldak (Ref. 8) and Tekriwal and Mazurnder (Ref. 10) have assumed a cut-off temperature of 600°C (1112°F) in their works. Without a cut-off temperature, the model becomes unstable and gives excessive deflections. The cut-off temperature of 750°C is selected since the model assumes zero value of yield strength at temperatures beyond 750°C.

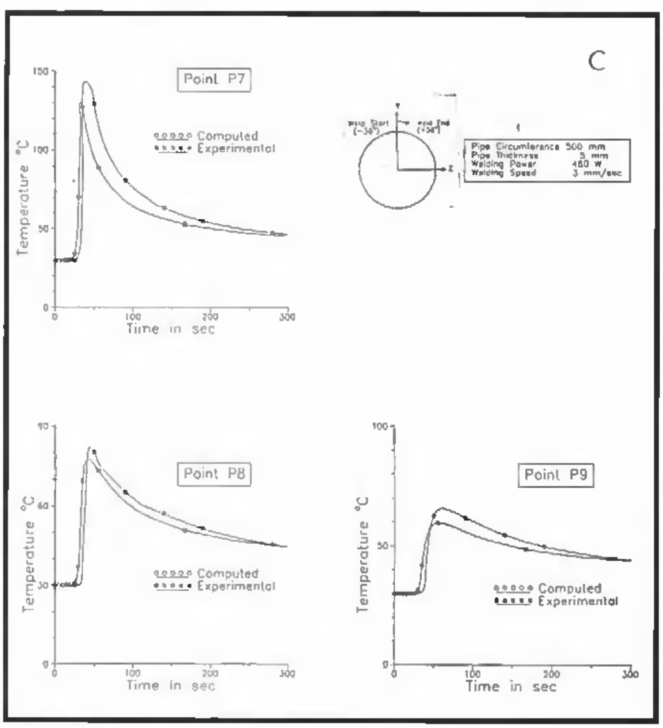

Fig. 13 — C — comparison of thermal cycles in the partially welded pipe.

Two computer programs have been developed for the analysis of transient thermal history and displacement history of the pipes (Ref. 24). The programs are written in C language and run on a PC with 80486 configuration and a clock speed of 25 MHz. Due to the limitation of 640 kB RAM size for the computer, an out-of-core solution based on the method of substructuring is followed for handling problems of reasonable size.

Experimental Validation

Experimental Trials

For validating the developed models, experiments have been conducted on a 160 mm (6.3 in.) diameter (circumference of 500 mm(20 in.), 5 mm (0.2 in.) thick carbon steel pipe conforming to the ASTM standard SA 135 Grade B (Ref. 24). As the measurement of axis shift distortion in a fully welded pipe is difficult, the welding has been conducted only for a circumferential segment of 100 mm (4 in.) on the pipe. Prior to welding, the pipes with machined edges have been tack welded only in the 100-mm segment marked for welding. The length of each tack weld is kept to a minimum, and the total length of the three tack welds is only 12 mm (0.5 in.). The tack-welded pipe is shown in Fig 6, but it has been noted that even in the tack-welded condition, there is a significant root opening in the opposite segment. This value has been accurately measured using feeler gauges as shown in Fig. 7.

After tack welding, chromel alumel thermocouples with a diameter of 0.5 mm (0.02 in.) are affixed at nine locations on the surface of the pipe as shown in the developed view of the pipe surface in Fig. 8 (Refs. 24, 25). The thermocouples are connected to a multichannel digital data acquisition system, which acquires and records the temperature data from thermocouples at an interval of 1 s.

The tack-welded pipe is mounted on a rotary positioner, and the gas tungsten arc welding (GTAW) setup employed for the trial is shown in Fig. 9. The speed of rotation is adjusted to obtain a linear welding speed of 3 mm/s (7 in./min). The GTAW process is employed without any filler metal, and the power input is 480 W. A lower value of power input is employed to avoid any possible melt through. The arc has been initiated without the conventional high-frequency start, as this might affect the data acquisition system. After the arc is initiated using touch start, the rotary positioner is activated and the welding on the pipe is performed. The temperature data are recorded up to a time of 400 s from the weld start time.

After the complete cooling of the pipe, the root opening at the bottom of the pipe is found to open out as shown in

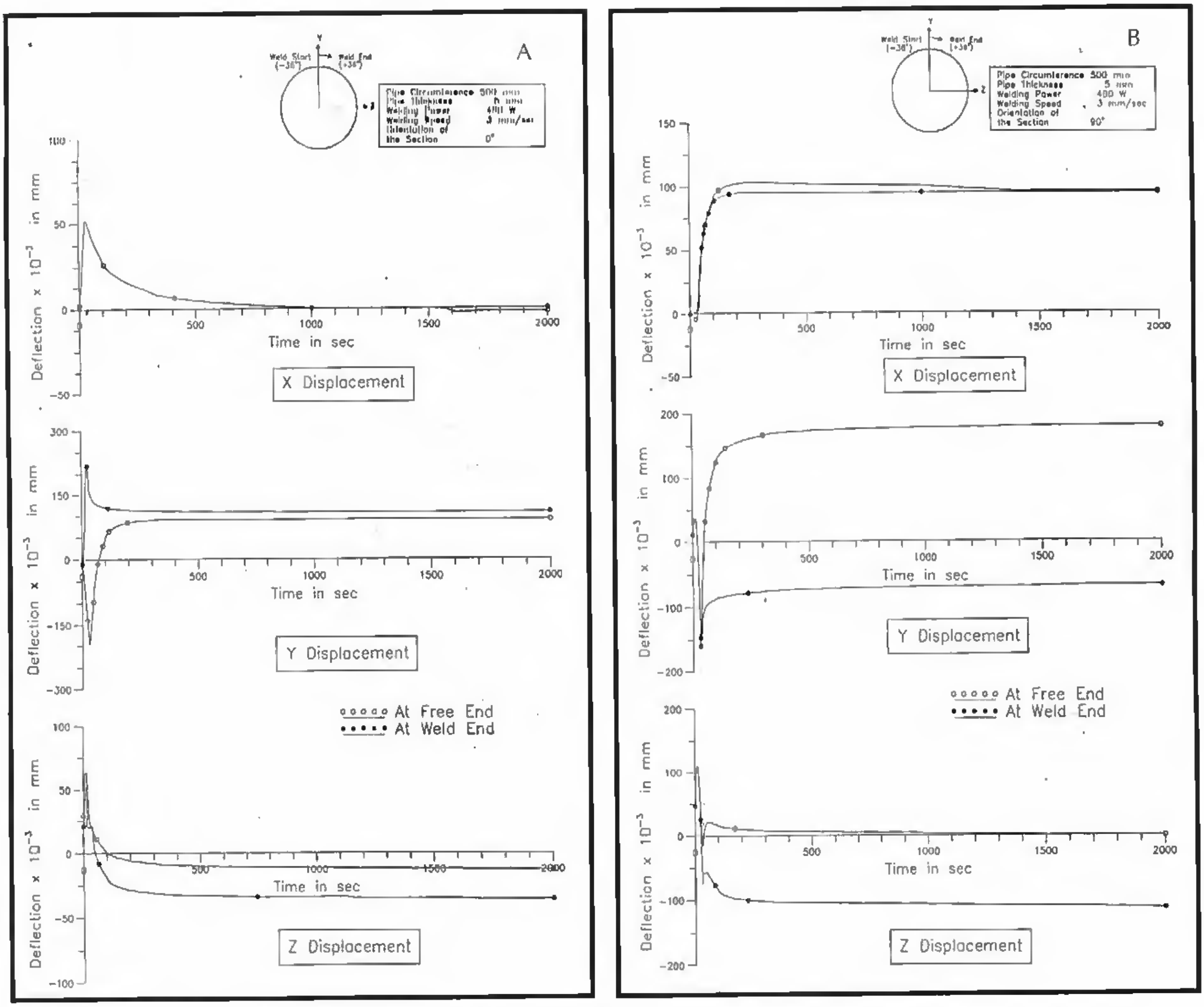

Fig. 14 — A — Transient displacement history in the partially welded pipe; B — transient displacement history in the partially welded pipe.

Fig. 10. This opening is measured accurately with the help of feeler gauges after welding. To eliminate any experimental error and to ensure consistency, the trial was repeated on one more set of pipe.

Thermal and Stress Analyses

The thermal and stress analyses were performed for the above case of partially welded pipe to validate the model. The thermal and stress analyses employ the four-noded bilinear degenerated shell element. The pipe is discretized as shown in Fig. 11, and the total numbers of nodes and elements are 360 and 324, respectively (Ref. 25). Due to the assumption of symmetry, only one-half of the pipe is taken for the analysis. The analysis assumes that the pipe is stationary during welding. The location at the 12 o'clock position is taken as 0-deg orientation. During welding, the arc moves from −36 deg, which is the weld start point, to +36 deg orientation, which is the weld end point.

The thermal problem is conducted for various time intervals, and the time step employed during the welding phase is 0.33 s, which corresponds to 1-mm (0.04-in.) movement of the arc for each step. After the completion of welding, the time interval is progressively increased up to a time of 2000 s when the pipe cools down to near room temperature. Subsequent to the thermal analysis, the stress analysis is performed. The size of the problem in stress analysis is 2160 as there are six nodal degrees of freedom for the element.

The boundary conditions adopted for the stress model are shown in Fig. 12. The condition assumes that the nodes lying in the weld interface on the plane of symmetry cannot move axially as the weld is intact and keeps the weld together. Thus, the axial movement of the nodes lying on the 100-mm weld segment are arrested. In addition, three more conditions are imposed to prevent any rigid body motion of the pipe. Additional boundary conditions have to be imposed during the welding period when the arc is moving along the circumference. During this time, due to the expansion of the pipe in the top segment, the points at the bottom segment try to move into the plane of symmetry as shown in Fig. 12, but actually this movement into the plane of symmetry is not possible. Hence during the welding period, the axial movement of all the points lying on the plane of symmetry is suppressed. However,

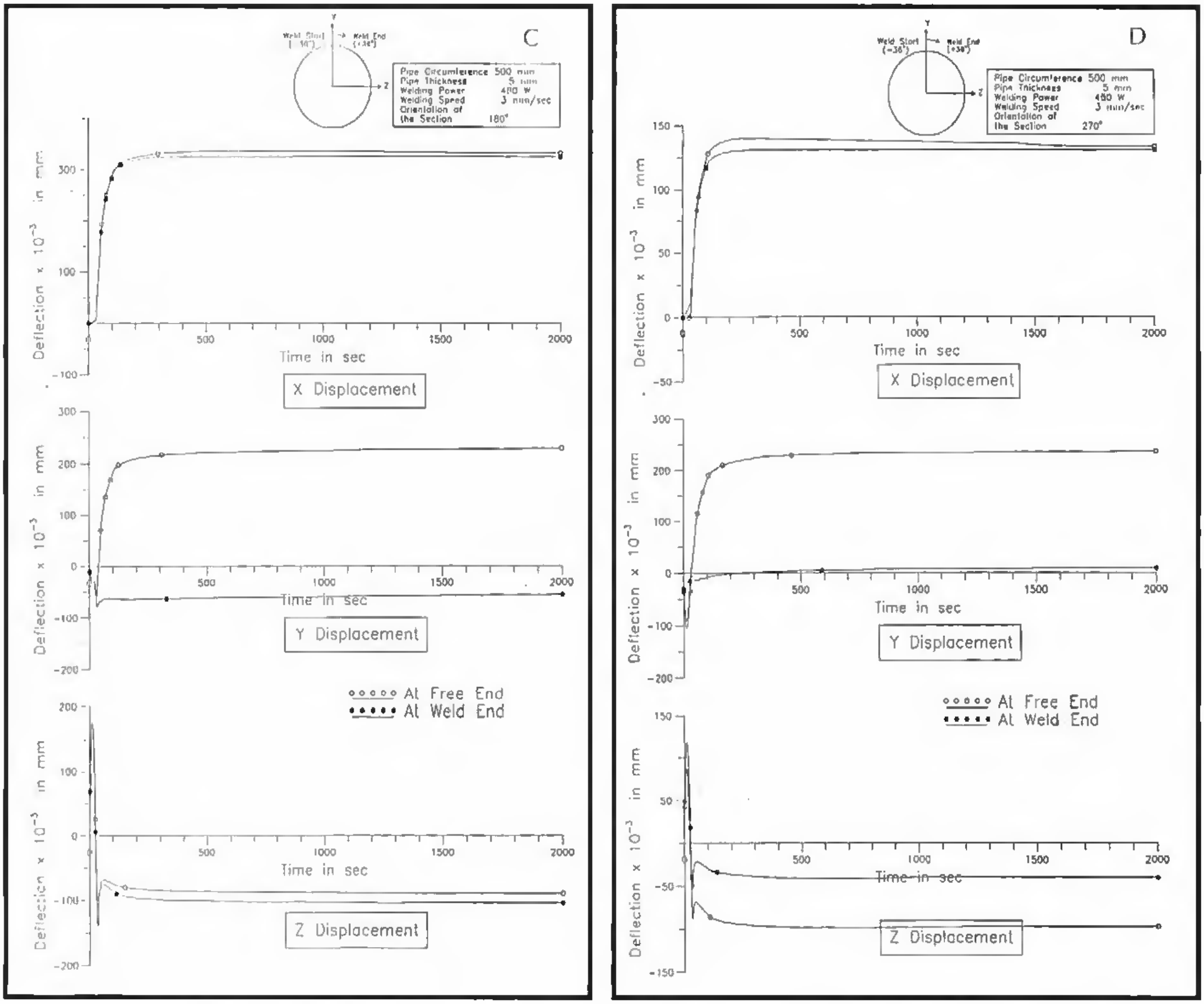

Fig. 14 — C — Transient displacement history in the partially welded pipe; D — transient displacement history in the partially welded pipe.

after the completion of welding, the pipe starts cooling and the movement of the bottom points will be in the opposite direction, *i.e.*, away from the plane of symmetry, and these additional boundary conditions are not applied during the cooling phase.

The analyses have been run using a PC with 80486 configuration and 25 MHz clock speed. The time taken by the PC for one step of thermal analysis is around 10–15 s, whereas the time taken for one step of stress analysis is nearly 45 min. As the time taken for the stress analysis is much higher compared to the time taken for thermal analysis, during the welding period, the stress analysis considers temperature distribution corresponding to every fifth time step during the welding time. In the cooling period when the shrinkage strains develop, the analysis is conducted every thermal step.

Results and Discussion

Thermal Results

The comparison between experimentally measured and computed temperature results for the nine locations are shown in Fig. 13A, B and C (Refs. 24, 25). The agreement is found to be good in most of the cases, The locations P1 and P2 are behind the starting point of the arc and get heated due to the backward flow of heat from the weld. While the agreement is good for point P1, at point P2 the computed results are less than the experimental values. This deviation is due to the unavoidable time lag between the initiation of the arc and the start of the rotary positioner, which results in more heat flow initially. This excess heat affects the results in point P2, but at a farther point P1, the effect is not felt much. Similarly, there is a deviation for the point P7, which lies ahead of the end point of welding, that can be attributed to the weld crater turbulence.

The thermal results for point P3, which is 5 mm from the weld interface, show that the computed results are less than the experimental values by about 24%. The deviation could be due to the uncertainties of thermal properties at high temperatures and the assumption in the model that the thermal gradient is negligible along the thickness for the shell element. Thus, the experimentally measured temperatures at the top surface of the pipe are higher than the average temperature computed at the midpoint along the thickness. For points P4, P5 and P6,

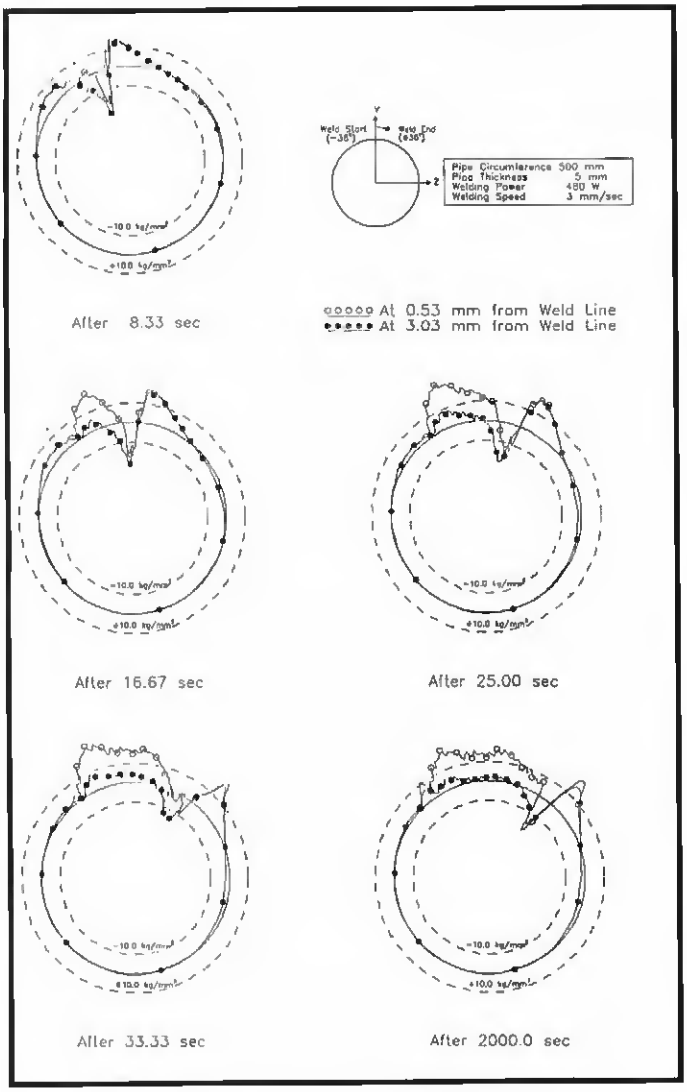

Fig. 15 — Circumferential distribution of axial stress in the partially welded pipe.

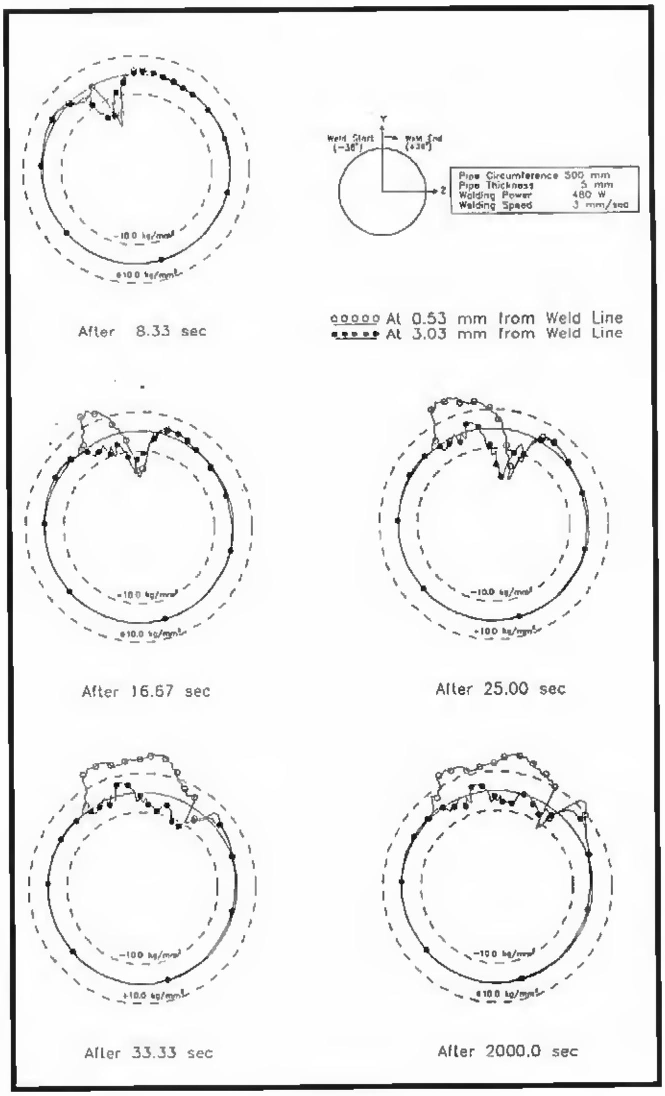

Fig. 16 — Circumferential distribution of circumferential stress in the partially welded pipe.

which are at 7.5, 17.5 and 27.5 mm (0.3, 0.7 and 1.1 in.) from the weld interface, the matching of the result is within 9, 7 and 4%, respectively. This agrees well with Ref. 7, which mentions that the stable thermal gradient for a pipe of 8-mm (0.35 in.) thickness is reached after 8 mm from the weld interface. The overall agreement between the computed and measured thermal results shows that the thermal model is validated.

Displacement Results

The experimental size of the opening at the bottom of the partially welded pipe is 1.75 and 1.9 mm (0.07 and 0.075 in.) for the first and second welding trials, respectively, whereas the corresponding root opening values after the tack-welded stage are 0.9 and 0.95 mm (0.035 and 0.037 in.), respectively. Thus, the deflection of the pipes due to welding is only 0.85 (0.033 in.) and 0.95 mm, respectively, giving an average value of 0.9 mm. The deflection value obtained from theoretical study for one symmetrical half is 0.324 mm (0.012 in.) , giving a total deflection value of 0.648 mm (0.025 in.). The results are of the same trend, and the agreement in the magnitude is of the order of 72%.

The deviation between the predicted and experimentally measured results could be due to the increased heat input, especially at the start and end of welding, caused by the time delay between the arc striking and the positioner rotation. In addition, the coarse mesh and the uncertainties in material properties at high temperatures could also have caused the deviation. However, the correlation between the computed and experimental values is reasonably good, which shows that the elastic-plastic model is validated.

The transient deflections in the X, Y and Z directions at four sections along the circumference of the pipe are shown in Fig. 14A, B, C and D. In each graph, the deflection history at the free end of the pipe, along with the corresponding deflection history for the weld joint end, is given. The graph reveals that the deflection in the axial direction (denoted as the X direction) in all orientations, except the 0-deg orientation, is nearly zero initially, during the heating phase (up to a time of 33 s), but once the arc heating is over, the deflections at the 90-, 180- and 270-deg segments (3 o'clock, 6 o'clock and 9 o'clock positions, respectively) rise rapidly to the steady-state value. In the 0-deg segment, the free end has a positive

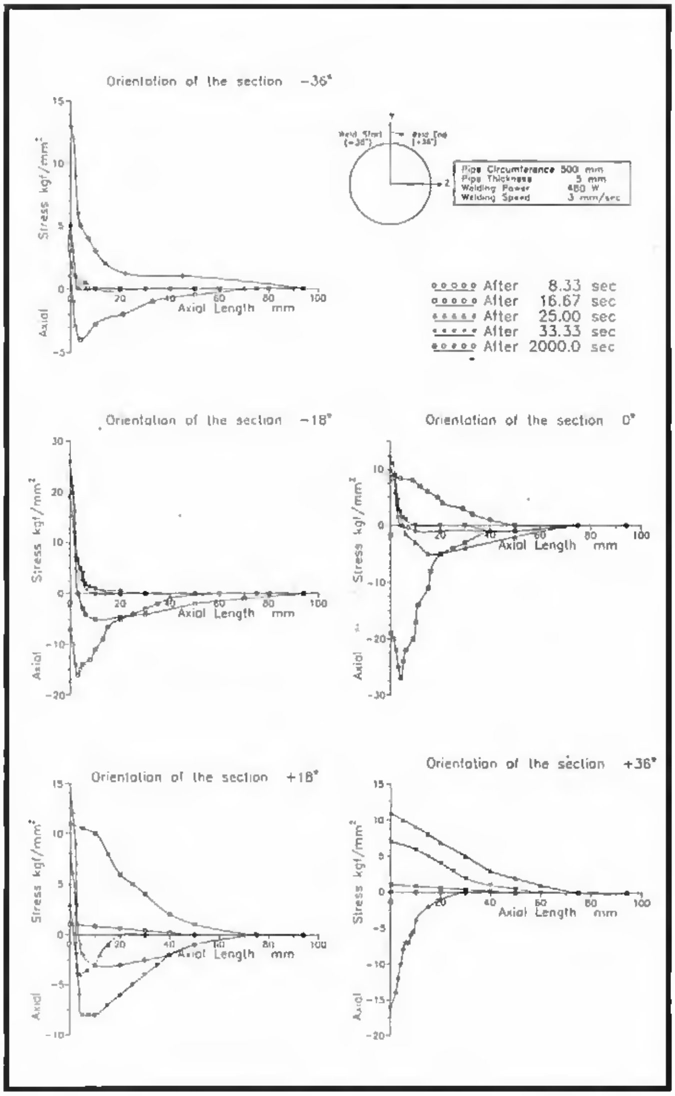

Fig. 17 — Axial distribution of axial stress in the partially welded pipe.

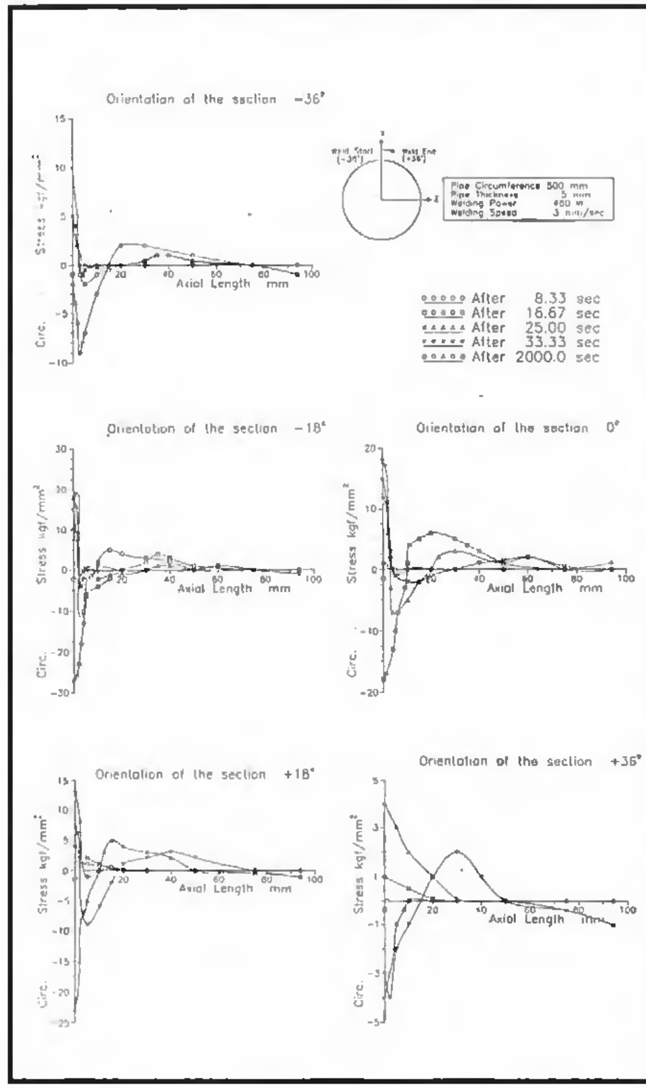

Fig. 18 — Axial distribution of circumferential stress in the partially welded pipe.

deflection value during heating but the value comes nearly back to zero after complete cooling. The deflection in the 0-deg orientation is in response to the arc heating, and the zero deflection in other locations is due to the boundary conditions assumed in the model.

The transient Y and Z deflections for the above orientations are also given in the figures. It is seen that the Y movement (vertical movement) in the 0-deg orientation at the free end and at the weld end is of opposite trend during the welding period. During this period, the free end moves down due to the thermal expansion in the top layers and, as a result, the weld end moves up because of the boundary conditions that are applied to the weld start and stop points (*i.e.*, −36-deg and +36-deg orientations). In the 180-deg orientation, both the weld end andthe free end move down during the heating period due to the thermal expansion of the pipe. But during cooling, the free end moves to the positive Y direction with the weld end remaining on the negative side. The trends in the 90-deg segment and 270-deg segment are not identical with the steady-state Y deflection in the free end, being negative for the 90-deg segment and near zero for the 270-deg segment.

The Z displacement (horizontal movement) at all the points is in the positive direction as the welding starts in the −36-deg orientation, and the thermal expansion of the pipe causes the movement the of free end in the positive Z direction. As the arc crosses the 0-deg orientation, the trend is reversed, and the movement is in the negative direction. This is due to the combined effect of expansion in the positive Z segments and shrinkage in the negative Z segments. After cooling the deflection remains on the negative side.

Thermal and Residual Stress Results

The axial and circumferential stresses are determined at the Gauss points, which lie in the local r-s plane, and the circumferential distribution of axial and circumferential stresses for various time intervals is shown in Figs. 15 and 16, respectively. The stresses are compressive at the point of welding and tensile at the locations that have been covered by the arc. After complete cooling, the stresses in the weld region are tensile, and in the rest of the pipe, the stresses are negligible. The stresses close to the weld are of high magnitude, but at 3 mm (0.12 in.) from the weld, the stresses are signifi-

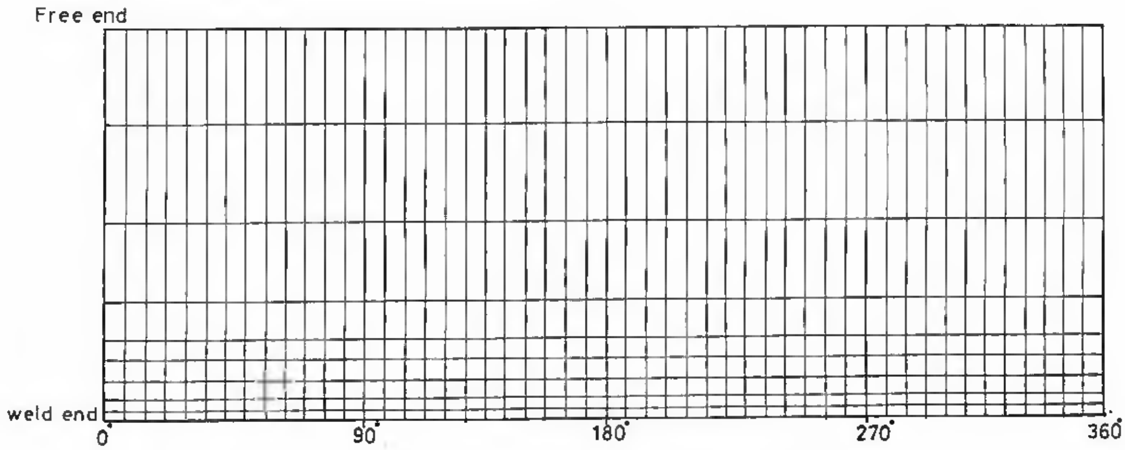

Fig. 19 — Discretization of the fully welded cylindrical pipe (developed view).

cantly less. The trend of the circumferential stress is also similar to that of the axial stress. The circumferential distribution of the axial stresses does not violate the equations of equilibrium as the equations of equilibrium in the theory of elasticity state that the condition of equilibrium is achieved by the combined action of normal and shear stresses. The degenerated shell element takes the transverse shear stresses into consideration, and hence, there is no violation of the equations of equilibrium.

The axial variation of the axial stress and the circumferential stress at various segments along the circumference for various time intervals is presented in Figs. 17 and 18, respectively. The trend is similar in both cases. Compressive stresses are induced when the arc is crossing a location, and after cooling, the stresses become tensile. The trend is, however, opposite in the weld end point (+36-deg orientation). The axial variation of the stress is gradual when the section is heated by the arc, but after cooling, the axial variation is very steep and points beyond 20 mm (0.8 in.) from the weld have negligible residual stresses.

Analysis of a Pipe Welded Circumferentially

To analyze the axis shift distortion in the case of fully welded pipe, the analysis has been conducted on a pipe having a circumferential length of 250 mm (10 in.) and a wall thickness of 1 mm (0.04 in.). The material of the pipe is assumed to be carbon steel having the thermal characteristics as given in Fig. 3. Figure 19 shows the discretization adopted for the pipe. Due to the assumption of symmetry, only one-half of the pipe is taken for the analysis. The discretization is the same for both the thermal and stress analyses. The total number of nodes and elements are 500 and 450, respectively. The analysis assumes that the pipe remains stationary during the circumferential welding and that the welding arc travels around the pipe in the clockwise direction. The weld is assumed to start from the 12 o'clock position, which is taken as the 0-deg orientation. The welding process is assumed to be GTA with an arc energy of 500 W and a welding speed of 1 mm/s (2.4 in./min).

The thermal analysis is conducted using a time increment of 1 s for the period when the arc travels around the circumference. After the completion of welding, the time increment is increased progressively up to a time of 3800 s and the analysis is conducted for a total of 300 thermal steps.

Subsequent to the thermal analysis, the elastic-plastic stress analysis is conducted on the pipe to determine the axis shift distortion. The same discretization as the one used for the thermal analysis is employed here, and the total number of nodes and elements are 500 and 450, respectively. But the total size of the problem is 3000, as there are six nodal degrees of freedom. The boundary conditions followed for the stress analysis are given in Fig. 20. The axial movement of all the nodes lying on the plane of symmetry is suppressed. In addition, three more conditions are imposed in the Y and Z directions to prevent any rigid body motion of the pipe. The boundary conditions imply that the pipe is tack welded securely before welding and the tack welds prevent any movement of the nodes lying on the plane of symmetry.

As the time taken for the stress analysis is much higher compared to the time taken for the thermal analysis, the stress

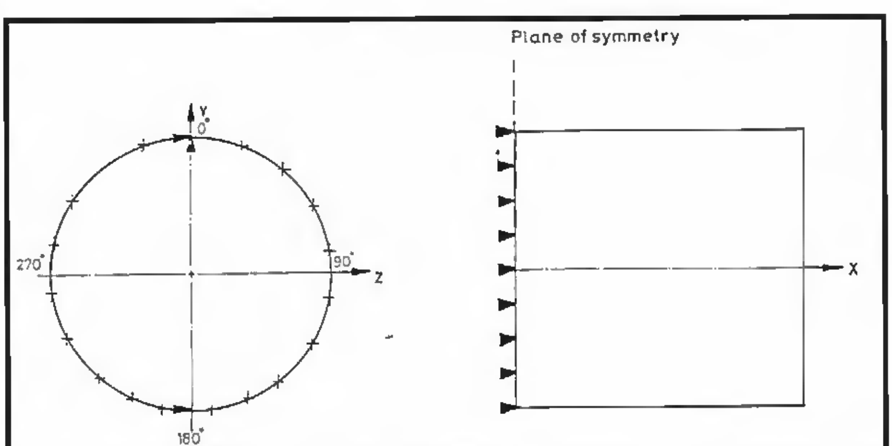

Fig. 20 — Boundary conditions employed for the fully welded cylindrical pipe.

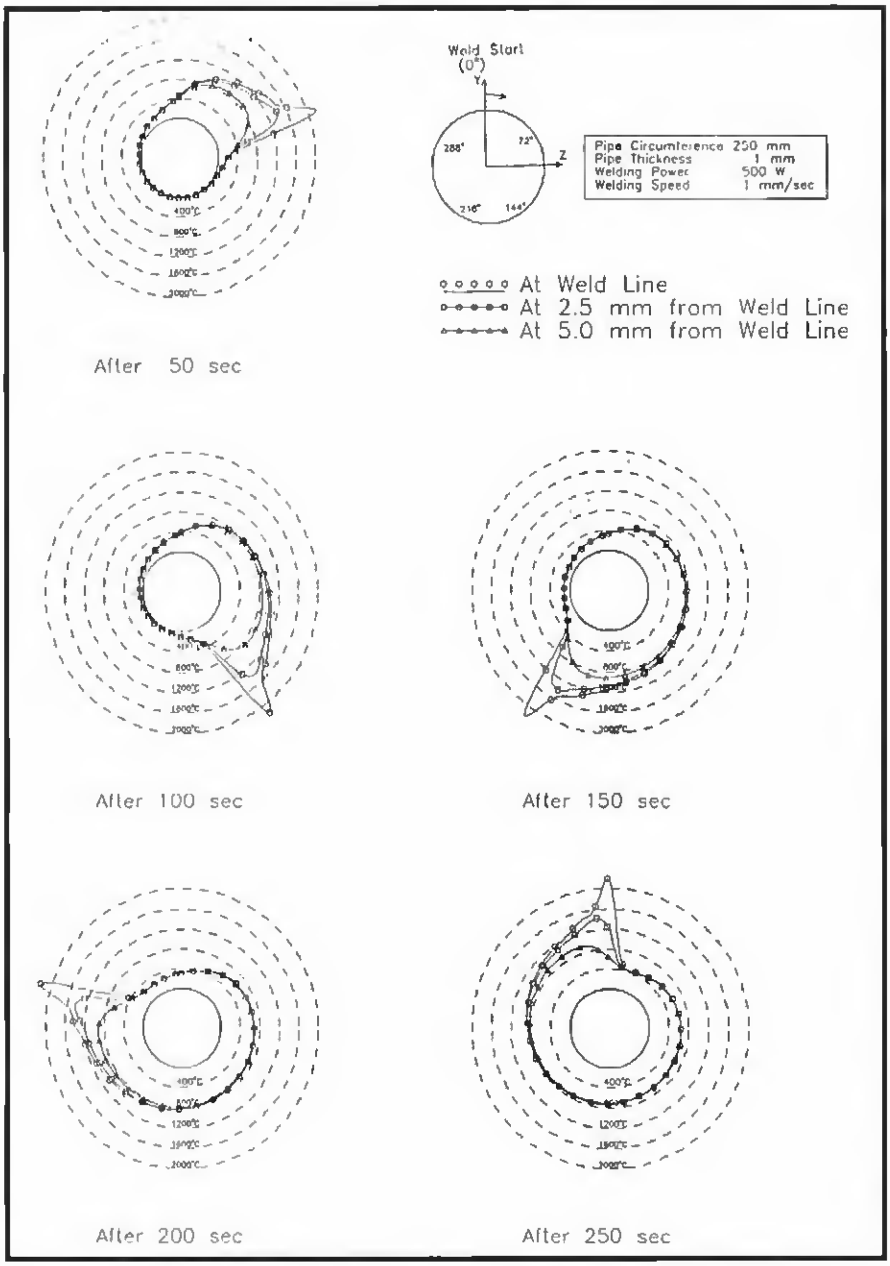

Fig. 21 — Circumferential temperature distribution in the fully welded cylindrical pipe.

analysis is performed by taking every fifth set of temperatures during the welding phase. However, during the cooling phase, the stress analysis is conducted at each thermal step. Thus, there are totally 100 steps for the stress analysis. The analyses have been run using a PC with 80486 configuration and 25 MHz clock speed. The time taken by the PC for one step of thermal analysis is around 10–15 s, whereas the time taken for one step of stress analysis is nearly 60 min. Thus, for the complete elastic-plastic analysis of circumferentially welded cylindrical pipe, the total time taken is nearly 100 h on the personal computer.

Results and Discussion

Thermal Results

Figure 21 shows the circumferential temperature distribution corresponding to weld line at 2.5 mm from the weld interface and 5 mm from the weld for various time intervals (Ref. 25). The temperature distribution shows that the peak temperatures are experienced at a point on the weld when the arc crosses that point. The temperature gradient ahead of the arc is very steep, whereas the gradient behind the arc is steep to begin with but less steep later, indicating fast cooling of the weld initially and slower cooling later.

The temperature distribution at a section away from the weld centerline is similar in trend but with less magnitude. The peak temperatures drop exponentially from the weld line along the axial direction. The thermal gradients ahead and behind the peak position at locations away from the weld line are not as steep, as in the case corresponding to the weld line. Similarly, the time for peak temperature also varies with distance from the weld. At the weld centerline, the peak temperature occurs at the time when the arc crosses that section. But at some distance away, the peak occurs some time after the arc has crossed the section. The temperatures in the weld around the circumference are not uniform when the arc has nearly covered one rotation. But at a distance of 5 mm from the weld interface, the temperatures are more uniform when the arc is about to complete one rotation.

The analysis is able to predict the flow of heat in the backward direction also. The thermal cycles at the 288-deg orientation reveal significant preheating effect, which is only marginal for the previous sections. Thus, the analysis is able to compute the temperature at all points in the pipe for various time intervals successfully.

Displacement Results

The results of the transient deflection at the free and weld ends at various segments along the circumference in the three directions are shown in Fig. 22A–E. The result for axial deflection (denoted as the X direction) for a plane at 0 deg, as shown in Fig. 22A, shows that the rate of the movement is high initially but that the rate gradually comes down as the section cools down. But as the arc approaches the plane once again toward the end of welding, the rate of the axial movement increases once again. After the welding is completed at 250 s, the rate still increases due to the conduction of heat from the weld and falls gradually thereafter, reaching a slightly negative value in the end. The axial movement at the 144-deg, and 216-deg segments shows that the deflection starts after some time lapse, which is the time lag for the arc to approach the plane. But the segment at 288 deg does not show this lag due to the heat received from the backward flow from the arc and the deflection in the 0-deg orientation.

The deflection at the free end in the Y direction shows that the movement is cyclic during the welding phase. The movement is negative to begin with

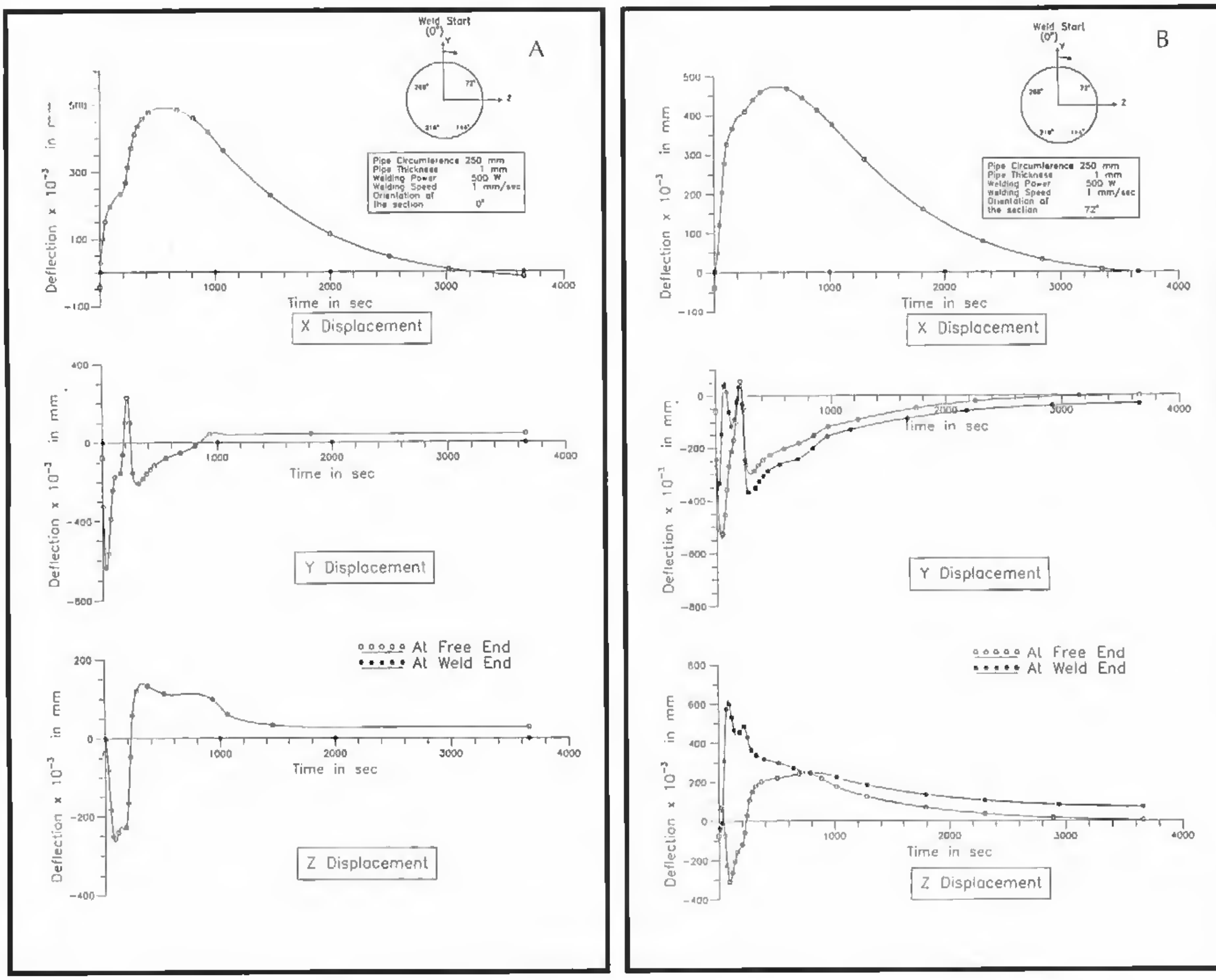

Fig. 22— A — Transient displacement history in the fully welded cylindrical pipe; B — Transient displacement history in the fully welded cylindrical pipe.

when the arc is at the 12 o'clock position. But when the arc comes to the 6 o'clock position, the trend is reversed and the movement is in the positive Y direction. When the arc goes to the 12 o'clock position again, the trend is once again negative. The initial displacement trend at the weld end is in the negative Y direction due to thermal expansion, but subsequently the trend for the weld end is just opposite to that for the free end, as shown in the figures.

The explanation for the difference between the behavior for the weld end and that for the free end is that when the arc is present at the 12 o'clock position, the top layers expand and, as a result, the pipe experiences a bending moment. Due to this moment, the free end at the bottom segment moves down but the weld end in the bottom segment moves up. Similarly when the arc comes down, the free end at the bottom layer moves up while the weld end moves down. But once the welding is completed, the bottom segment moves down due to the thermal expansion and the trend of the weld end thereafter is similar to that of the free end. After complete cooling, the free end has some differential Y displacement with respect to the weld end.

Similar behavior is experienced for the Z deflection also, but here the trend at the free end is negative for a longer time, *i.e.*, from the time when the arc is at the 12 o'clock position to a time when the arc is at the 6 o'clock position. When the arc moves further, the trend in the Z deflection is reversed. The behavior of the weld end during this period is opposite to that of the free end as in the case of Y deflection.

The deflections in the Y and Z directions corresponding to the weld end and free end show variations until about 1000 s. Beyond 1000 s, the difference in the deflections between the weld end and the free end remains steady. Beyond that time the two deflections move back toward the zero value as the pipe cools down and the thermal strain value becomes smaller.

The peak value of the Y deflection in the 144-deg and 216-deg orientations is slightly more than that in the 72-deg and 288-deg orientations. This is because of the boundary conditions assumed in the model, which assume the point in the 0-deg orientation to be fixed. Hence, due to thermal expansion of the pipe, the points in the lower side move down to a greater extent. Similarly, the peak Z deflection of the 72-deg and 288-deg ori-

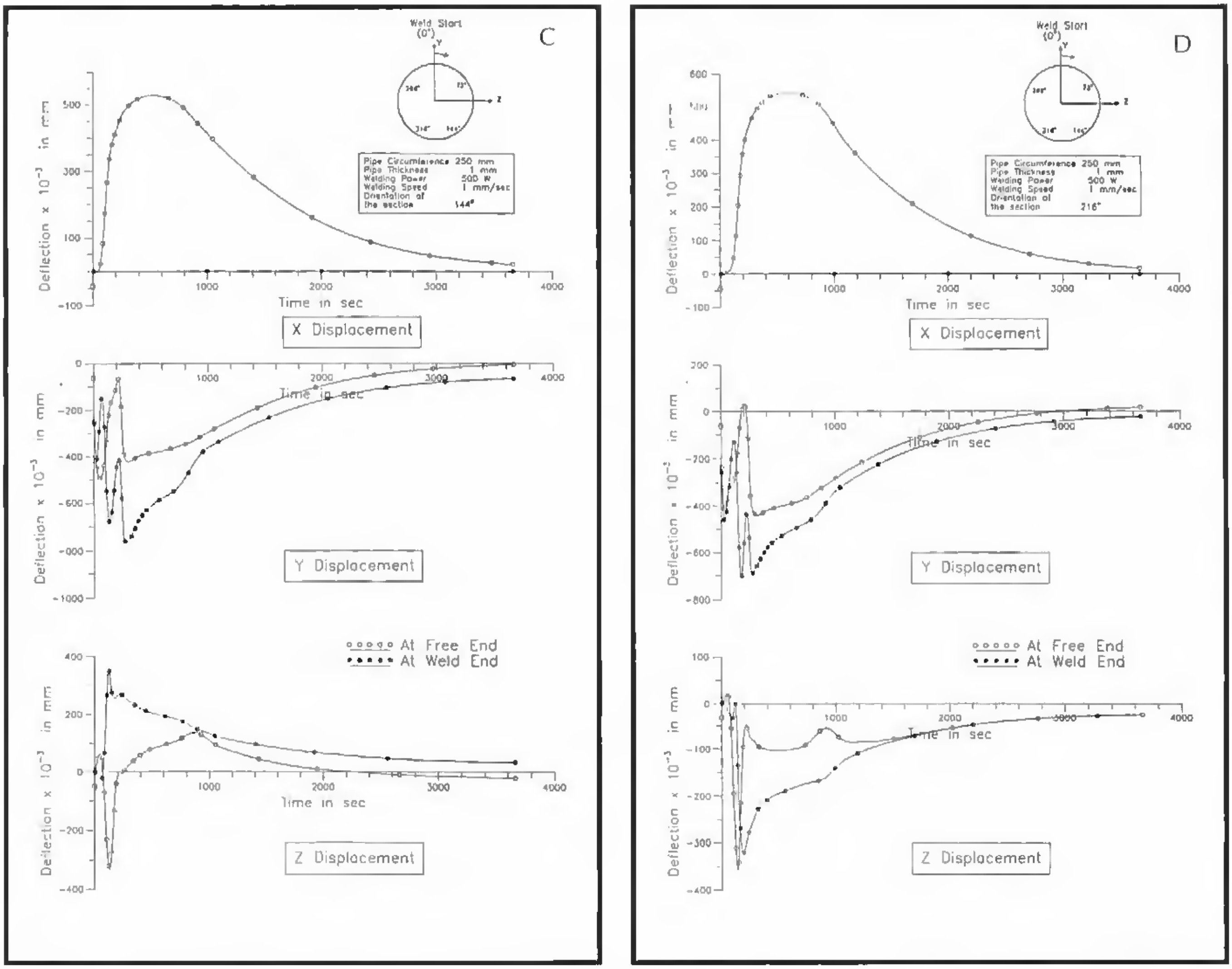

Fig. 22— C — transient displacement history in the fully welded cylindrical pipe; D — transient displacement history in the fully welded cylindrical pipe.

entations is more than the values for the 144-deg and 216-deg orientations. This is due to the higher Z coordinate value for the 72-deg and 288-deg segments.

Thermal and Residual Stress Results

The circumferential distribution of the axial stresses for sections closest to the weld at various time intervals shows that the stresses in the welded region are zero when the temperature remains higher than the cut-off temperature of 750°C. Once the point cools down below the cut-off temperature, stresses of tensile nature are induced in the weld.

The arc region is heated up rapidly, but, due to the higher temperatures, the stresses are also lower. However, at points ahead of the arc, which are still at temperatures close to the ambient value, high tensile stresses are induced due to the expanding metal in the arc region. In a small region behind the weld start point, the flow of heat in the backward direction causes compressive stresses due to the constraints on the expanding metal by the surrounding metal. Beyond this region, tensile stresses are induced in the initial period up to about 100 s. This is due to the bending of the pipe due to arc heating. Beyond 100 s, the stress in this region becomes less. The final steady-state residual axial stress distribution is not axisymmetric as shown in the figure.

The circumferential distribution of the stresses for sections closest to the weld at various time intervals shows that the magnitude of the circumferential stress is much less than that of the axial stress. This shows that the pipe offers little restraint for the thermal expansion in the circumferential direction. After complete cooling of the pipe, unlike the axial stresses, the circumferential stresses are more or less axisymmetric, except in the weld start location. This is in agreement with the experimental finding in Ref. 16. The circumferential stresses in the weld after complete cooling are compressive, which has also been reported in Ref. 7.

Conclusions

A finite element methodology has been successfully developed for the analysis of axis shift distortion and stress buildup during the circumferential welding of thin-walled, large-diameter pipes. The analyses have been successfully performed using a four-noded bilinear degenerated shell element. The satisfac-

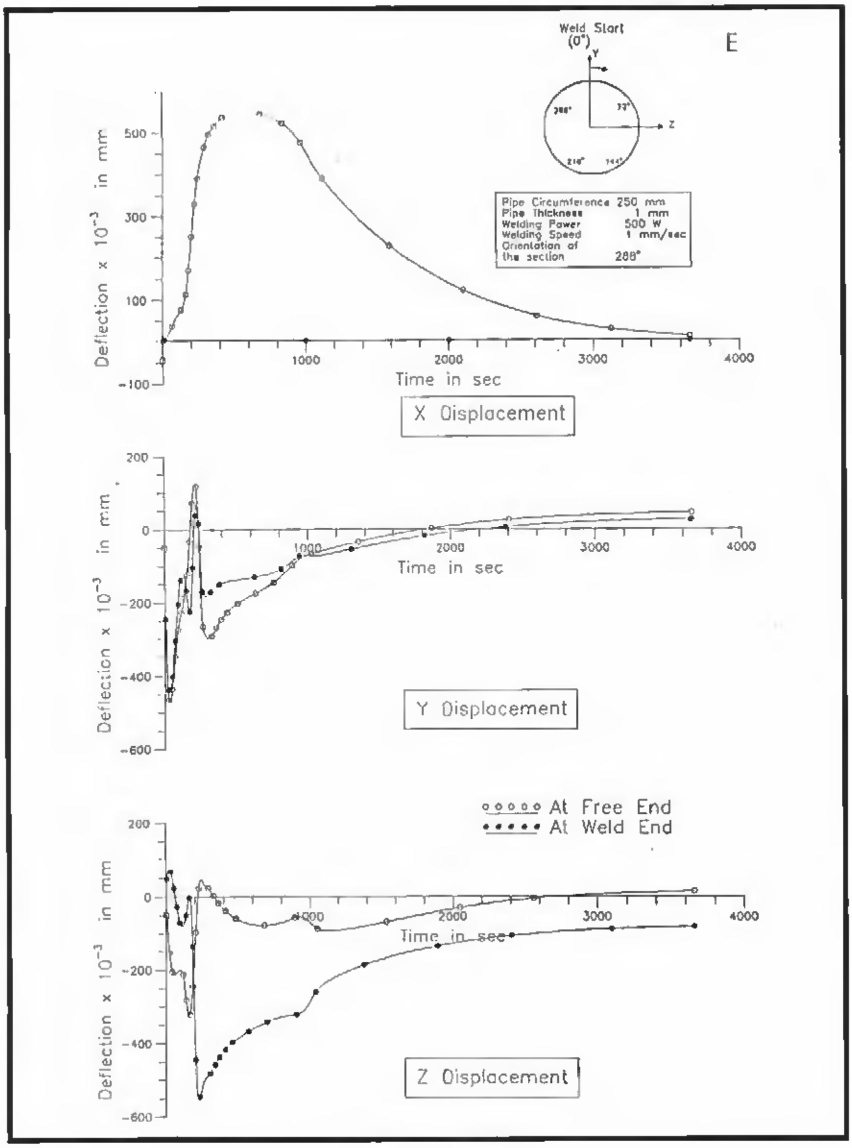

Fig. 22— E — transient displacement history in the fully welded cylindrical pipe.

tory performance of the shell element shows that the assumption made by the element, *viz.*, that the gradient of the field variables (temperature and stress) is negligible in the local thickness direction, is reasonable for the cases analyzed. The validation of the thermal results through experiments conducted on the partially welded pipe shows that the various phenomena are reasonably incorporated in the model. The deviation between the predicted and computed temperatures decreases gradually with distance from the weld. The agreement between the predicted and experimentally measured opening in a partially welded pipe shows the efficacy of the elastic-plastic stress model. The transient displacement history in the case of a fully welded pipe shows that the pipe exhibits bending behavior due to the arc heating. The movement at the weld end and the free end shows differences, which ultimately manifest as axis shift distortion of the pipe. The circumferential residual stress field is more uniform around the circumference than the axial residual stress field.

Acknowledgment

The authors wish to express their sincere gratitude to the management of BHEL for the constant encouragement at various stages of this work and for their permission for the publication of this work.

References

1. Gurunathan, T., Wilfred, S., Arunagiri, S., and Mazumdar, S. K. 1987. Statistical analysis of deviation caused by weld distortion during manufacture of nuclear steam generators. *National Welding Seminar,* Bangalore, India, pp. B1–B10.

2. Friedman, E. 1975. Thermomechanical analysis of welding process using finite element method. *Transactions of ASME Journal of Pressure Vessel Technology* 97(3): 206–213.

3. Krutz, and Segerlind, L. J. 1978. Finite element analysis of welded structures. *Welding Journal* 57(7): 211-s to 216-s.

4. Goldak, J., Bibby, M., Moore, J., House, R., and Patel, B. 1986. Computer modeling of heat flow in welds. *Metallurgical Transactions B.* 17B: 587–600.

5. Kannatey-Asibu, E., Jr., Kikuchi, N., and Jallad, A-R. 1989. Experimental finite element analysis of temperature distribution during arc welding. *Transactions of ASME, Journal of Engineering Materials and Technology* 111: 9–18.

6. Goldak, J., McDill, M., Oddy, A., House, R., Chi, X., and Bibby, M. 1986. Computational Heat Transfer for Weld Mechanics. *Proceeding of International Conference on Trends in Welding Research,* Ed. S. A. David. ASM International, Materials Park, Ohio, pp. 15–20.

7. Karlsson, R. I., and Josefson, B. L. 1990. Three dimensional finite element analysis of temperatures and stresses in a single pass butt welded pipe. *Transactions of ASME, Journal of Pressure Vessel Technology* 112: 76–84.

8. Goldak, J., Oddy, A., McDill, M., Chakravarti, I. A., Bibby, M., and House, R. 1986. Progress in Computing Residual Stress and Strain in Welds. *Proceedings of International Conference on Trends in Welding Research,* Ed. S. A. David, ASM International, Materials Park, Ohio, pp. 523–527.

9. Leung, C. K., Pick, R. J., and Mok, D. H. B. 1990. Finite element modeling of a single pass weld. WRC Bulletin 356, pp. 1–10.

10. Tekriwal, P., and Mazumder, J. 1991. Transient and residual thermal strain stress analysis of GMAW. *Transactions of ASME, Journal of Engineering Materials and Technology* 113: 336–343.

11. Vaidyanathan, S., Todaro, A. F., and Finnie, I. 1973. Residual stresses due to circumferential welds. *Transactions of ASME, Journal of Engineering Materials and Technology* 95: 233–237.

12. Vaidyanathan, S., Weiss, H., and Finnie, I. 1973. A further study of residual stresses in circumferential welds. *Transactions of ASME, Journal of Engineering Materials and Technology* 95: 238–242.

13. Rybicki, E. F., Schmueser, D. W., Stonesifer, R. W., Groom, J. J., and Mishear, H. W. 1978. A finite element model for residual stresses and deflections in girth butt welded pipes. *Transactions of ASME, Journal of Pressure Vessel Technology* 100: 256–262.

14. Scaramangas, A. 1984. Residual stresses in girth butt welded pipes. Technical Report No. CUED/D-Struct/TR 107. Department of Engineering, Cambridge University.

15. Chandra, U. 1985. Determination of residual stresses due to girth butt welds in pipes. *Transactions of ASME, Journal of Pressure Vessel Technology* 107: 178–184.

16. Jonsson, M., and Josefson, B. L. 1988. Experimentally determined transient and residual stresses in a butt welded pipe. *Journal of Strain Analysis,* 23(1): 25–31.

17. Lingren, L., and Karlsson, L. 1988. Deformations and stresses in welding of shell

structures. *International Journal for Numerical Methods in Engineering* 25: 635–655.
18. Josefson, L., Jonsson, M., Karlsson, L., Karlsson, R., Karlsson, C. T., and Lindgren, L. E. 1989. Transient and residual stresses in a single pass butt welded pipe. *International Conference on Residual Stresses*, ICRS-2, Eds. G. Beck, S. Denis and A. Simon, Elsevier Applied Science, London, U.K., pp. 497–503.
19. Worsak, K. N. 1979. A simple and efficient finite element for general shell analysis. *International Journal for Numerical Methods in Engineering* 14: 179–200.
20. Segerlind, L. J. 1984. *Applied Finite Element Analysis*, John Wiley and Sons, Inc.
21. Krishnamoorthy, C. S. 1987. *Finite Element Analysis-Theory and Programming*, Tata McGraw Hill Publishing Co. Ltd.
22. Bathe, K. J. 1982. *Finite Element Procedures in Engineering Analysis*, Prentice Hall, Inc.
23. Linnert, G. E. 1967. *Welding Metallurgy Carbon and Alloy Steels, 3d ed.*, Vol. 2, American Welding Society, Miami, Fla., pp. 108–117.
24. Ravichandran, G. 1995. Analysis of Axis Shift Distortion and Residual Stresses during Circumferential Welding. Ph D Thesis. Indian Institute of Technology, Madras, India.
25. Ravichandran, G., Raghupathy, V. P., Ganesan, N., and Krishnakumar, R. 1995. Prediction of temperature distribution during circumferential welding of thin pipes using finite element method. *International Journal for the Joining ofMaterials* 7(1): 34–44.

4th International Seminar Numerical Analysis of Weldability

September 29–October 1, 1997

Chairman H. Cerjak

Co-Chairmen H. K. D. H. Bhadeshia, B. Buchmayr

Invitation to Participation and Call for Papers

The deadline for the submission of abstracts is **April 1, 1997**; the abstract should be sent to the seminar chairman. Extensive articles with a substantial review content are particularly welcome, since one of the conference aims is to establish authoritative literature that is of lasting value and sufficiently detailed to help newcomers to the field.

If you are interested in presenting a paper, please send an abstract of not more than one-half page containing title of the paper, name of the author(s), and affiliation to the seminar chairman no later than **April 1, 1997.**

The seminar subcommittee will inform you by **May 1, 1997,** about the acceptance of your paper.

The final paper has to be sent to the chairman by **September 1, 1997,** by mail, fax or email (bernie@weld.tu-graz.ac.at).

For more information, contact

Chairman H. Cerjak, TU Graz
Attn: Bernhard Schaffernak
Abteilung Werkstoffkunde und Schweißtechnik
Kopernikusgasse 24, A-8010 GRAZ, Austria
Tel. No.:+43-316/873-7182, Fax No.:+43-316/873-7187
World Wide Web: http://www.cis.tu-graz.ac.at/weld/seggau.html